In Vitro and In Vivo Tracer Characteristics of an Established Multidrug-Resistant Human Colon Cancer Cell Line

Dietrich E. Lorke, Matthias Krüger, Ralph Buchert, Karl H. Bohuslavizki, Malte Clausen, and Udo Schumacher

Departments of Neuroanatomy and Nuclear Medicine, University Hospital Eppendorf, Hamburg, Germany

^{99m}Tc-methoxyisobutylisonitrile (^{99m}Tc-MIBI) has been suggested as a tracer for the scintigraphic detection of multidrug resistance (MDR). The aim of this study was to compare MDR characteristics in vitro and in vivo by immunohistochemic and functional uptake assays in established tumor cell lines cultured and grown in severe combined immunodeficient (SCID) mice. **Methods:** The presence of MDR was assessed in vitro in drug-resistant HT-29^{mdr1} colon carcinoma cells and in nonresistant HT-29^{par} cells by JSB-1 immunohistochemistry, uptake of the fluorescent dye Rhodamine 123, and quantitative measurement of ^{99m}Tc-MIBI accumulation. For in vivo imaging, SCID mice bearing subcutaneous xenografts of these cell lines were injected with ^{99m}Tc-MIBI and ^{18}F-FDG for scintigraphic and PET examination. After imaging, tumors were analyzed by immunohistochemistry and electron microscopy. **Results:** All HT-29^{mdr1} cells cultured in vitro exhibited distinct JSB-1 immunoreactivity, although to a variable degree, whereas HT-29^{par} cells were completely devoid of JSB-1 staining. Rhodamine 123 accumulated poorly in HT-29^{mdr1} cells but strongly in HT-29^{par} cells. Accumulation of ^{99m}Tc-MIBI was 0.05% ± 0.01% of the activity of the external medium in HT-29^{mdr1} cells, but about eight times higher in HT-29^{par} cells (0.40% ± 0.09%), a very low percentage compared with other tumor cell lines. No difference in ^{201}TlCl accumulation was observed between both cell lines. In vivo, neither HT-29^{par} nor HT-29^{mdr1} tumors grown in SCID mice could be detected by ^{99m}Tc-MIBI scintigraphy. In FDG PET, both HT-29^{mdr1} and HT-29^{par} tumors were clearly visible. FDG uptake was, however, markedly higher in HT-29^{par} than in HT-29^{mdr1} tumors. Both tumor types were poorly vascularized, as shown histologically. JSB-1 immunoreactivity was absent in all HT-29^{par} tumors examined, whereas the majority of HT-29^{par} tumor cells were stained. Electron microscopy showed that HT-29^{par} tumors contained significantly less mitochondria than hepatocytes of the SCID mouse liver, which displayed high ^{99m}Tc-MIBI uptake in our scintigraphy studies. **Conclusion:** Sufficient ^{99m}Tc-MIBI uptake is the major prerequisite for distinguishing successfully between drug-resistant and sensitive cells. Negative ^{99m}Tc-MIBI scintigrams are not necessarily associated with MDR expression. In some tumors, FDG may be an in vivo marker for MDR as suggested by PET.

Key Words: human HT-29 colon cancer cell line; electron microscopy; FDG; PET; immunohistochemistry; multidrug resistance; Rhodamine 123; severe combined immunodeficient mouse; ^{99m}Tc-methoxyisobutylisonitrile; ^{201}TlCl

J Nucl Med 2001; 42:646–654

O ne major obstacle in the chemotherapeutic treatment of cancer patients is the emergence of tumor cells resistant to anticancer agents. The lack of response often develops in tumors, which initially have responded well to chemotherapy, simultaneously involving various different chemotherapeutic agents, such as anthracyclins (e.g., doxorubicine), alkaloids (e.g., vincristine, colchicine), and epipodophyllotoxins (VP-16). This acquired resistance to a wide range of unrelated drugs is referred to as multidrug resistance (MDR). The mechanism most frequently involved is the overexpression of a 170-kDa plasma membrane phosphoglycoprotein, P-gp, encoded by the MDR1 gene (*1,2*). P-gp acts as a transmembrane energy-dependent drug-efflux pump that transports several apparently unrelated organic compounds, such as cytostatics, out of the cell, resulting in drug resistance (*3*).

To design the most efficient therapy protocols and to reduce unwanted secondary effects of chemotherapy to a minimum, it is of great clinical importance to predict the outcome of cancer therapy by identifying those patients that will not respond to anticancer treatment. ^{99m}Tc-methoxyisobutylisonitrile (^{99m}Tc-MIBI) is a suitable transport substrate of P-gp, and its cellular accumulation is inversely proportional to the level of P-gp expression (*4,5*). It has therefore been hypothesized that functional in vivo imaging with ^{99m}Tc-MIBI may allow the rapid characterization of P-gp expression in tumors (*5*). This procedure would permit us to assess the efficacy of chemotherapy and thus to select appropriate chemotherapy regimens. In fact, several reports suggest that tumors with higher ^{99m}Tc-MIBI uptake are more likely to respond to chemotherapy than those with a lower uptake (*6,7*). Other studies, however, indicate that ^{99m}Tc-MIBI imaging is not useful for predicting the response to chemotherapy (*8*). Further investigations suggest

that P-gp expression is not exclusively related to initial ^{99m}Tc-MIBI uptake, but rather to the washout of ^{99m}Tc-MIBI from the tumor (9).

These contradictory results may, in part, be related to the fact that different forms of human tumors have been studied. We have therefore chosen an established human colon carcinoma cell line (HT-29) and its MDR counterpart (10–12) to study P-gp expression by the same cancer cell line in vitro and in vivo. The severe combined immunodeficient (SCID) mouse model allows the systematic analysis of in vivo characteristics of human tumors growing in the microenvironment of a living organism (13,14). Human cancer cells cultured in vitro are transplanted into SCID mice, which lack functional B and T lymphocytes. In this system, tumor cells retain the morphology and functional characteristics of the original tumor and thereby rather accurately reflect the clinical situation (14).

Our purpose was to determine P-gp expression of nonresistant and MDR HT-29 human colon carcinoma cell lines both in vitro by immunohistochemic and functional assays and in vivo by functional imaging using ^{99m}Tc-MIBI and ^{18}F-FDG in the same carcinoma cells growing in SCID mice. We then compared these results with histologic and electron microscopic analyses.

MATERIALS AND METHODS

Cell Culture

The human colon carcinoma cell line HT-29^{par} was obtained from the American Type Culture Collection through the European Tissue Culture Collection (Porton Down, Salisbury, U.K.). The MDR HT-29^{mdr1} cell line (10) was generously supplied by Dr. I. N. Slotki (University of Jerusalem, Israel). Cells were cultivated to confluence in 50-mL tissue culture flasks under standard conditions (37°C, 100% relative humidity, 5% CO_2/95% air) in McCoy's 5A medium (Gibco/Life Technologies, Karlsruhe, Germany), supplemented with 10% heat-inactivated fetal calf serum ([FCS] Gibco), 2-mM L-glutamine, 100 U/mL penicillin, and 100 μg/mL streptomycin (cell culture medium). In addition, for maintaining the HT-29^{mdr1} cell line, 300 ng/mL colchicine was added to the culture medium. Because substantial numbers of cells were necessary to standardize and reproduce the experiments, cells were subcultured and cryopreserved in a cryo-safe I (c.c. pro GmbH, Neustadt, Germany) medium in multiple identical aliquots. Before each experiment, cells were thawed and incubated for 7 to 14 d in the culture medium.

For immunohistochemic detection of MDR, HT-29^{par} and HT-29^{mdr1} cells cultivated on Chamber Slides (Nunc, Naperville, IL) were rinsed in 0.1 mol/L phosphate-buffered saline ([PBS] 4°C, pH 7.4) and then fixed in 4% paraformaldehyde in 0.1 mol/L phosphate buffer (1 h, 4°C, pH 7.4). After several rinses in PBS, cells were processed for immunohistochemistry as described below.

In addition, MDR was visualized by an assay based on an increased rate of fluorescent dye efflux in MDR cells, resulting in reduced staining (15). After cultivation for 48 h on Chamber Slides, HT-29^{par} and HT-29^{mdr1} cells were incubated for 10 min with 5 μg/mL Rhodamine 123 (Sigma, Munich, Germany) in the culture medium (37°C, 5% CO_2). To exclude different mechanisms of reduced Rhodamine uptake, the MDR transporter was inhibited by adding 10 μg/mL weak detergent Tween 80 (Fluka, Buchs, Switzerland) to the medium in control incubations. After several rinses in the cell culture medium, coverslips were placed over the slides using Crystal Mount plus Clarion Permanent Mounting Media (Biomeda Corp., Foster City, CA), examined immediately, and photographed under a Zeiss Axiophot fluorescence microscope (Carl Zeiss, Oberkochem, Germany).

Uptake of ^{99m}Tc-MIBI In Vitro

For quantitative assessment of the MDR transporter function, ^{99m}Tc-MIBI was applied to cultured tumor cells, and its uptake was compared with that of ^{201}TlCl (DuPont Pharma, Brussels, Belgium). Synthesis of ^{99m}Tc-MIBI was performed with a one-step kit formulation (Cardiolite; DuPont, Bad Homburg v.d.H., Germany) as described by Piwnica et al. (16). Radiochemical purity was ≥95%, as measured by thin-layer chromatography using aluminum oxide plates (1B-F; JT Baker, Phillipsburg, NJ).

Adherent cells were harvested with 0.05% trypsin/0.53-mM EDTA (Gibco) and washed once in the culture medium. After a recovery period (incubation for 2 h at 37°C; 5% CO_2), cells were counted on a Neubauer hemocytometer (Optik Labor, Friedrichshofen, Germany), suspended in the same serum-free medium at a concentration of 0.3×10^6 cells/mL, and distributed into 18 test tubes each (for HT-29^{par} and HT-29^{mdr1} cells), 3 mL per tube. Two test tubes containing the culture medium, but no cells, served as control tubes.

A volume of 50 μL ^{99m}Tc-MIBI, dissolved in 0.9% NaCl to a final concentration of 20 kBq/50 μL, was added to nine test tubes and one control tube. Specific activity of ^{99m}Tc taken from the generator was about 1 MBq/nmol; that is, the total amount of MIBI was about 20 pmol/10^6 cells, which is far below saturation (17). The remaining nine test tubes and the remaining control tube were incubated with 50 μL ^{201}TlCl and dissolved in 0.9% NaCl to a final concentration of 20 kBq/50 μL. The specific activity of ^{201}Tl was about 0.7 MBq/nmol; that is, the total amount of ^{201}TlCl was about 30 pmol/10^6cells. After an incubation period of 1 h (37°C, 5% CO_2), tracer uptake by the cells was stopped by adding 7 mL ice-cold water, thus limiting the duration of exposition to the tracers to a defined period. After three rinses in ice-cold PBS (5 min at 1,500 rpm), cell pellets were suspended in 1 mL ice-cold PBS in Eppendorf tubes (Eppendorf, Hamburg, Germany). The radioactivity of the pellets was determined in a gamma well counter (FH 412; Frieseke & Hoepfner, Erlangen-Bruck, Germany). The Eppendorf tubes were measured for 1 min within the ^{99m}Tc energy window and for 1 min within the ^{201}Tl energy window (window width, 40–100 mV; high voltage at maximum counting rate). Measured counting rates were corrected for background and radioactive decay. To obtain relative tracer uptake, the counting rate of the cell probes was divided by the counting rate of the appropriate control probe. The two-tailed Student t test for unpaired data was used to evaluate statistical differences between the tracer uptake of HT-29^{par} and HT-29^{mdr1} cells. The t test was performed for equal (homoscedastic) or unequal (heteroscedastic) variances according to the result of Levene's test.

To minimize nonspecific binding of ^{99m}Tc-MIBI to plastic or metal surfaces, glassware was used whenever possible. Plastic pipette tips were presaturated with freshly prepared 1% bovine serum albumin (A9645; Sigma, Deisenhofen, Germany) in 0.1 mol/L PBS for 1 h (pH 7.4) followed by three washes in PBS (17).

Animals

Twenty-one male adult (10–14-wk-old) pathogen-free BALB/c SCID mice were used in this study. Principles of laboratory animal care (NIH publication no. 86–23, revised 1985) were followed, as well as the German Law on Animal Protection from 1987, and the local health ethics committee approved the experiments. Animals were kept in filter-top cages and were provided with sterile water and standard food (ssniff M-Z Alleindiät extrudiert; ssniff Spezialdiäten GmbH, Soest, Germany) ad libitum. All manipulations were performed aseptically under a laminar flow hood. For injection, HT-29^{par} and HT-29^{mdr1} cells were harvested by trypsinization and tested for viability (95%) after a culture period of 7–14 d, and 5×10^6 viable cells were resuspended in 1 mL McCoy's 5A medium (Gibco). Each recipient SCID mouse was injected subcutaneously with 200 μL of the cell suspension into the back between the scapulae; 12 animals received HT-29^{par} and 9 animals received HT-29^{mdr1} cells. When solid tumors had grown to a size of 1–1.5 cm^3 (after 3 wk for HT-29^{par} and after 5 wk for HT-29^{mdr1}), the animals underwent various imaging procedures.

Uptake of ^{99m}Tc-MIBI In Vivo

In each SCID mouse, about 200 μL ^{99m}Tc-MIBI, dissolved in 0.9% NaCl to a final concentration of 100 MBq/200 μL, were administered in the tail vein using a 1-mL Luer syringe (Braun, Melsungen, Germany) with a Microlance canula (Becton Dickinson, Dublin, Ireland). Planar scintigraphic images with a pixel size of 1.0×1.0 mm^2 were acquired over 15 min at 15 and 60 min after injection of ^{99m}Tc-MIBI. Each image was taken from the posterior view using a single-head gamma camera (Diacam; Siemens Medical Systems, Hoffman Estates, IL) equipped with a low-energy high-resolution parallel-hole collimator. To avoid artifacts caused by movement, mice were anaesthetized with 0.09 mg pentobarbital (Nembutal; Sanofi, Munich, Germany). Images were analyzed visually.

Uptake of FDG In Vivo

Thirty minutes after scintigraphy with ^{99m}Tc-MIBI, approximately 20 MBq glucose analog FDG (in-house production) were administered by intraperitoneal injection to 12 SCID mice; three carried an HT-29^{par} tumor and nine carried an HT-29^{mdr1} tumor. To monitor the time course of FDG uptake by the tumor, a dynamic series of 12 frames (duration 5 min each) was acquired immediately after tracer application using a conventional, full-ring, whole-body PET (ECAT EXACT 921/47; CTI/Siemens, Knoxville, TN). Transversal images with pixels of 0.7×0.7 mm^2 were reconstructed by filtered backprojection using a Shepp-Logan filter with a cutoff of 1.0 in units of the Nyquist frequency, leading to an in-plane resolution of 6.5 mm (full width at half maximum). Photon attenuation within the mice was neglected. To evaluate the uptake of FDG, the last four frames of the dynamic series were added, corresponding to a static acquisition from 40 to 60 min past injection. Transversal, coronal, and sagittal slices were analyzed visually on the computer monitor. To enable direct visual comparison with the results of the planar ^{99m}Tc-MIBI scintigraphy, maximum intensity projections from the posterior view were computed from the tomographic FDG PET slices.

Histology

After completion of the scintigraphy and PET, animals were killed by cervic dislocation. Tumors were excised within their capsule and cut into two pieces, one of them for paraffin wax histology and the other for electron microscopy. For paraffin histology, tissue specimens were immersion-fixed in 4% paraformaldehyde in 0.1 mol/L phosphate buffer (48 h, 4°C, pH 7.4), rinsed in 0.1 mol/L phosphate buffer (4°C, 12 h), dehydrated routinely, and embedded in paraplast using xylene as an intermedium. 5-μm coronal sections were mounted, rehydrated, and rinsed twice in PBS.

Immunohistochemistry. HT-29^{par} and HT-29^{mdr1} cells cultivated on Chamber Slides and fixed thereafter (see above), as well as rehydrated paraffin sections of tumors grown in SCID mice, were processed for immunohistochemic visualization of P-gp. After preincubation for 20 min in 10% normal swine serum diluted in antibody diluent (S-3022; Dako, Carpinteria, CA), slides were incubated for 1 h (20°C) in primary monoclonal antibody JSB-1 (No. MON 9011; Sanbio, Beutelsbach, Germany), diluted 1:100 in antibody diluent. After three rinses in 0.05 mol/L tris buffered saline ([TBS] pH 7.6), the tissue was incubated in biotinylated secondary antibody (LSABR2 Kit, K-0674; Dako, Carpinteria, CA) for 10 min (20°C), rinsed three times in TBS, and then incubated in streptavidin-alkaline phosphatase complex (LSABR2 Kit, Dako) for 30 min. Alkaline phosphatase activity was visualized after three washings in TBS by incubation in the substrate naphthol-AS bisphosphate supplemented with hexatozised New Fuchsine (Code No. 22931–8; Aldrich, Steinheim, Germany) for simultaneous coupling (20 min, room temperature). In addition, antilaminin (L-9393; Sigma, Steinheim, Germany) and antifactor VIII (Clone M 0616; Dako, Glostrup, Denmark) immunohistochemistry were used to visualize tumor blood vessels after the same staining protocol. The specificity of the immunoreactions was assessed by omission of either the primary or secondary antibody or the streptavidin-alkaline phosphatase complex, each resulting in negative staining. Slides were then rinsed, counterstained with hematoxylin, and mounted with Crystal Mount/Clarion (Biomeda).

Electron Microscopy. For ultrastructural examination, tissue specimens of about 4 mm^3 were taken from the tumors grown in SCID mice and immersed in a fixative consisting of 6% glutaraldehyde in 0.05 mol/L phosphate buffer (24 h, pH 7.3, 760 mOsm). The tissue was rinsed in a mixture of 0.1 mol/L phosphate buffer and 0.1 mol/L saccharose, postfixed with buffered osmium tetroxide (1% for 2 h), dehydrated in ethanol, cleared in propylene oxide, and embedded in glycidether 812 (Serva, Heidelberg, Germany). Then 1-μm-thick transverse semithin sections were cut with an OMU 3 ultramicrotome (Reichert, Vienna, Austria) and stained with toluidine blue and pyronine red. Ultrathin sections (70–90 nm) were prepared for electron microscopy and stained with saturated alcoholic uranyl acetate and lead citrate before examination with a CM100 transmission electron microscope (Phillips, Hamburg, Germany).

RESULTS

In Vitro Studies

Immunohistochemistry. P-gp expression of cell lines grown on coverslips was visualized by the use of the monoclonal antibody JSB-1. All HT-29^{par} cells were completely devoid of the anti-P-gp label (Fig. 1A). In contrast, almost all HT-29^{mdr1} cells were labeled distinctly, indicating the presence of P-gp (Fig. 1B). However, the intensity of the JSB-1 immunoreaction varied between individual cells. The majority of HT-29^{mdr1} showed a moderate to strong staining,
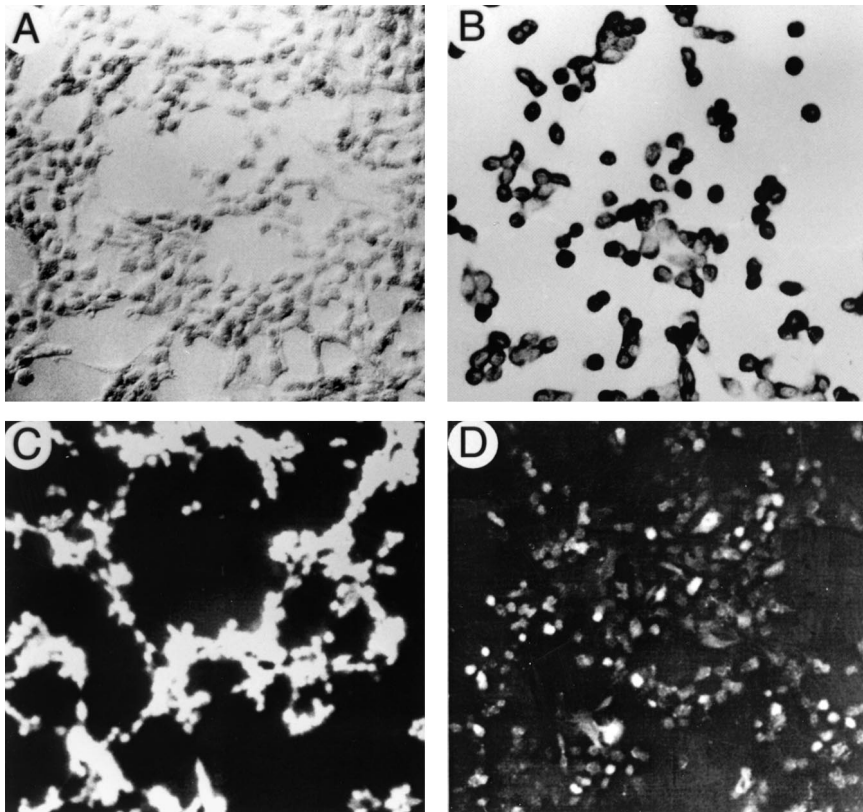
FIGURE 1. In vitro characteristics of HT-29par (A and C) and HT-29mdr1 (B and D) cell lines. Immunohistochemic visualization of P-gp expression: absence of label in HT-29par (A) and positive staining in HT-29mdr1 (B) cell lines. Functional assessment of P-gp was performed by Rhodamine 123 accumulation (C and D). Note bright fluorescence in HT-29par (C) cells in contrast to weak fluorescence in HT-29mdr1 cells (D) caused by increased efflux. Original magnification, ×450.

few cells were weakly positive, and <5% of the cells were completely unlabeled. The JSB-1 immunoreaction was most marked on the surfaces of the HT-29mdr1 cells.

Rhodamine 123 Uptake. MDR transporter activity was shown functionally by applying the fluorescent dye Rhodamine 123, which is taken up and retained by nonresistant cells but pumped rapidly out of the cytoplasm by the P-gp transporter protein in MDR cells (*15*). All HT-29par cells exhibited a bright fluorescent staining of varying intensity (Fig. 1C). In contrast, HT-29mdr1 cells showed only a very weak fluorescence; very few cells ($\leq$5%) exhibited strong Rhodamine 123 staining (Fig. 1D). Additionally, inhibition of the MDR transporter function by adding Tween 80 to the Rhodamine 123 incubation medium resulted in a marked increase in HT-29mdr1 cell fluorescence.

99mTc-MIBI Uptake. The MDR transporter function was assessed quantitatively in vitro by measuring the uptake of 99mTc-MIBI, which was significantly different in HT-29par and HT-29mdr1 cells ($P < 0.0001$). In HT-29par cells, 0.40% $\pm$ 0.09% (mean $\pm$ SD) of the activity of the external medium was detected after an incubation period of 1 h (Fig. 2). In contrast, in HT-29mdr1 cells, only 0.05% $\pm$ 0.01% was observed. 99mTc-MIBI uptake was therefore approximately eight times higher in HT-29par cells than in HT-29mdr1 cells.

In contrast, the uptake of 201TlCl, which is not a substrate of P-gp, was not significantly different in both cell lines ($P = 0.48$); 1.38% $\pm$ 0.12% and 1.34% $\pm$ 0.13% of the activity of the external medium were detected in HT-29par and HT-29mdr1 cells, respectively (Fig. 2). Both 99mTc-MIBI

and 201TlCl uptake essentially remained unchanged after incubation periods ranging from 1 to 4 h.

In Vivo Studies

Planar scintigraphic images of the SCID mice showed the physiologic distribution of 99mTc-MIBI, that is, uptake in the liver, urinary bladder, and intestine (Fig. 3). In addition, the injection site at the tail was visible in several animals. No significant difference in tracer uptake was observed between mice carrying HT-29par tumors (Fig. 3A) and those carrying HT-29mdr1 tumors (Fig. 3B). In addition, images obtained 15
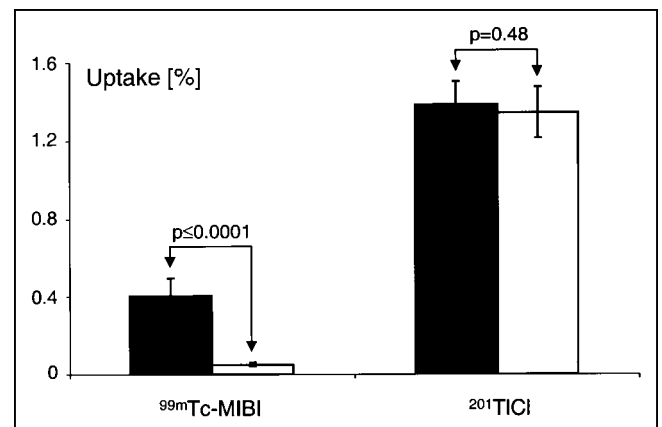

FIGURE 2. Uptake of 99mTc-MIBI and 201TlCl in HT-29par (black columns) and HT-29mdr1 (white columns) cells in percentage tracer in external medium. Data represent mean $\pm$ SD of nine cell suspensions each.
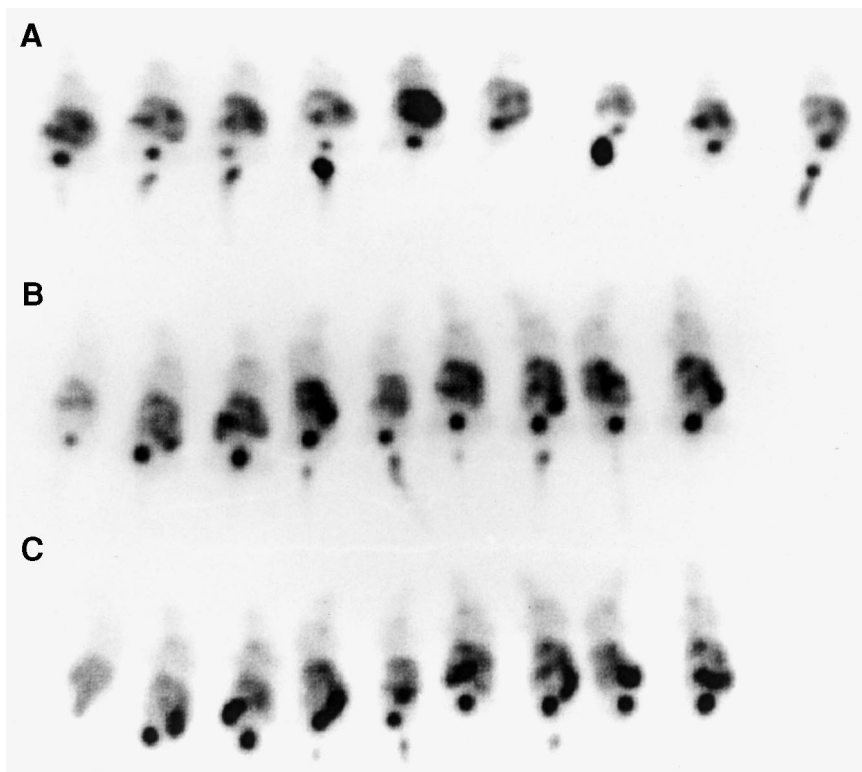
FIGURE 3. Planar scintigraphic images from posterior view obtained 15 min after injection of ^{99m}Tc-MIBI in SCID mice carrying HT-29^{par} (A) or HT-29^{mdr1} (B) xenografts between scapulae. Imaging of SCID mice carrying HT-29^{mdr1} tumors was repeated 60 min after injection (C). Upper threshold of color table was set to five times average tracer uptake in background. Physiologic tracer uptake is shown in liver, urinary bladder, and intestine. Tumors are not visible.

and 60 min after injection essentially were the same (Figs. 3B and C). Neither HT-29^{par} nor HT-29^{mdr1} tumors could be detected in any of the animals at any time examined.

In contrast, tumors were clearly visible in FDG PET (Fig. 4). All HT-29^{par} tumors and six of nine HT-29^{mdr1} tumors showed increased uptake of the glucose analog 60 min after injection, excluding the lack of tumor cell viability as a reason for negative ^{99m}Tc-MIBI imaging. Two of three HT-29^{par} tumors showed a very high uptake of FDG, whereas the uptake in the remaining HT-29^{par} tumor and in the HT-29^{mdr1} tumors for which the PET findings were positive was only moderately increased.

Histology

Both HT-29^{par} and HT-29^{mdr1} tumors examined after the imaging procedures were moderately differentiated, contained numerous mitoses, and displayed a sizable central necrosis. As visualized by antilaminin and antifactor VIII immunohistochemistry, both HT-29^{par} and HT-29^{mdr1} carcinomas were generally poorly vascularized. A marked regional variation in blood vessel distribution was observed, however (Fig. 5); blood vessels were located mainly in the tumor periphery close to the capsule, whereas very few vessels were found in its center. Immunohistochemical visualization of the P-gp showed an almost complete absence of JSB-1 immunoreaction in all HT-29^{par} tumors examined; <1% of the cells were weakly stained (Fig. 6A). In HT-29^{mdr1} carcinomas, a considerable variation between different cells in the JSB-1 label was observed. Overall staining intensity was much stronger than that of HT-29^{par} tumors,

however (Fig. 6B). In addition, as already observed in the cell culture, the intensity of the immunoreaction varied markedly between individual HT-29^{mdr1} cells in solid HT-29^{mdr1} tumors grown in SCID mice. Most HT-29^{mdr1} tumors were composed of cells showing weak, moderate, or strong JSB-1 immunoreaction; <5% of the cells were unlabeled. Few HT-29^{mdr1} carcinomas, however, contained up to 30% unlabeled cells. Generally, staining was observed in the cytoplasm of HT-29^{mdr1} cells. In addition, the membrane of numerous tumor cells was more strongly labeled than the cytoplasm. In differentiated areas of HT-29^{mdr1} and also in HT-29^{par} tumors, tumor cells were forming tubules with visible lumina. Remarkably, JSB-1 staining was confined to the luminal surface of these tubules.

Electron microscopy revealed that HT-29^{par} tumor cells showing almost no ^{99m}Tc-MIBI uptake in vivo contained only a few mitochondria (Fig. 7A), whereas hepatocytes of the SCID mouse, displaying high ^{99m}Tc-MIBI uptake in vivo, were packed densely with mitochondria (Fig. 7B).

DISCUSSION

This study compared in vitro and in vivo characteristics of the MDR colon carcinoma cell line HT-29^{mdr1} with those of the nonresistant tumor cell line HT-29^{par}. Before implantation into SCID mice, the MDR of the HT-29^{mdr1} cell line was ascertained in vitro by three different techniques: immunohistochemical visualization of the P-gp epitope using the JSB-1 antibody (*18*), functional assessment of the MDR efflux pump by Rhodamine-123 uptake studies (*15,19*), and
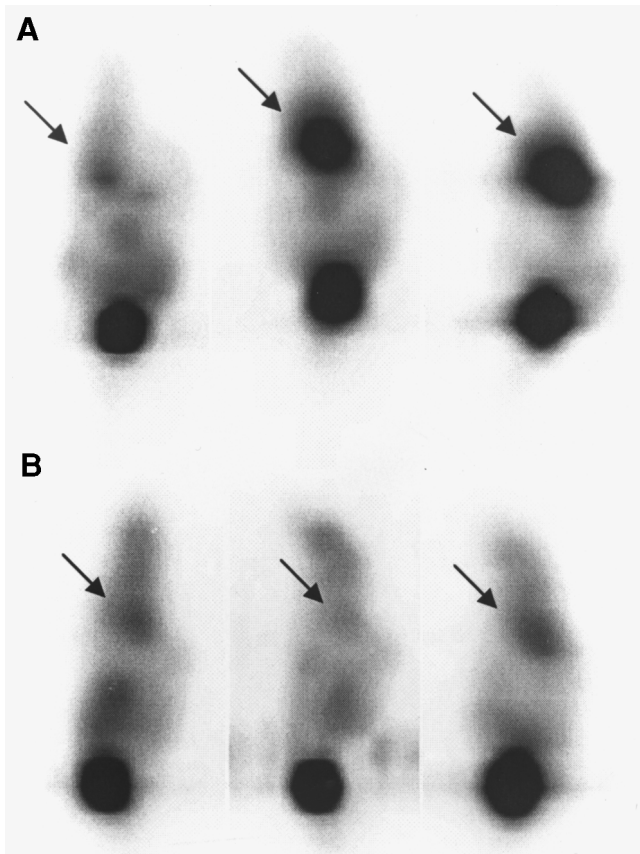
FIGURE 4. Maximum intensity projections from posterior view computed from transverse tomographic PET images acquired 50 min after injection of FDG in SCID mice carrying HT-29[par] (A) or HT-29[mdr1] (B) xenografts between scapulae. Uptake of glucose analog was increased significantly in all HT-29[par] tumors and in six of nine HT-29[mdr1] tumors (arrows).

This interindividual variation of P-gp expression in HT-29[mdr1] cells was also shown in our Rhodamine 123 accumulation studies. The fluorescent compound Rhodamine 123 is a known substrate for P-gp (19), and this property is exploited to detect MDR function using fluorescence microscopy. Rhodamine 123 staining in drug-sensitive cells is manifold higher than in MDR cells (15,19); it is not determined by the initial dye uptake, but rather by an efflux process (24). This active extrusion is directly correlated with the expression of P-gp, as observed in 58 cell lines in the National Cancer Institute drug screen (25). Thus, Rhodamine 123 accumulates passively within cells, driven in part by the negative plasma membrane potential (17,26), and drug-sensitive cells retain the dye, thereby remaining fluorescent for many hours. In drug-resistant cells, however, Rhodamine 123 is extruded by the P-gp, resulting in negative staining (15,24). The use of cytoplasmic exclusion of Rhodamine 123 as a functional assay for detecting the activity of the P-gp efflux pump in vitro has become a generally acknowledged technique in MDR research (27,28). In addition, recent clinical studies indicate that the Rhodamine 123 efflux assay is also of prognostic significance to predict the response to chemotherapy in acute leukemia (28,29). We have shown that HT-29[mdr1] tumor cells show essentially no accumulated fluorescence when compared with parental nonresistant cells, which are brightly fluorescent. These findings are in good agreement with previous studies showing that Rhodamine 123 efflux is markedly higher in HT-29[mdr1] than in HT-29[par] colon carcinoma cells (11,12).

quantitative evaluation of the P-gp drug transporter activity by measuring ^{99m}Tc-MIBI accumulation (4).

Our immunohistochemic data show that HT-29[mdr1] and HT-29[par] cell lines can be clearly distinguished immunohistochemically by binding of the JSB-1 antibody directed against the P-gp. Virtually all HT-29[mdr1] cells are immunoreactive, whereas a complete absence of label is observed in HT-29[par] cell lines. The specificity and sensitivity of the monoclonal antibody JSB-1 for detecting the P-gp on paraffin-embedded sections have been shown by Pavelic et al. (18). JSB-1 immunostaining was applied successfully in numerous studies to detect MDR cells (19–21) and, in some tumors, to predict the response to chemotherapy (22). Consistently, positive JSB-1 antibody plasma membrane staining for HT-29[mdr1] and the lack of immunoreactvity for HT-29[par] cell lines were reported previously by Spoelstra et al. (23). We found no differences between individual nonresistant HT-29[par] cells, which are all devoid of immunoreaction. However, the intensity of JSB-1 immunostaining varies between different HT-29[mdr1] cells, indicating that all MDR cells express the P-gp, but to a variable degree.
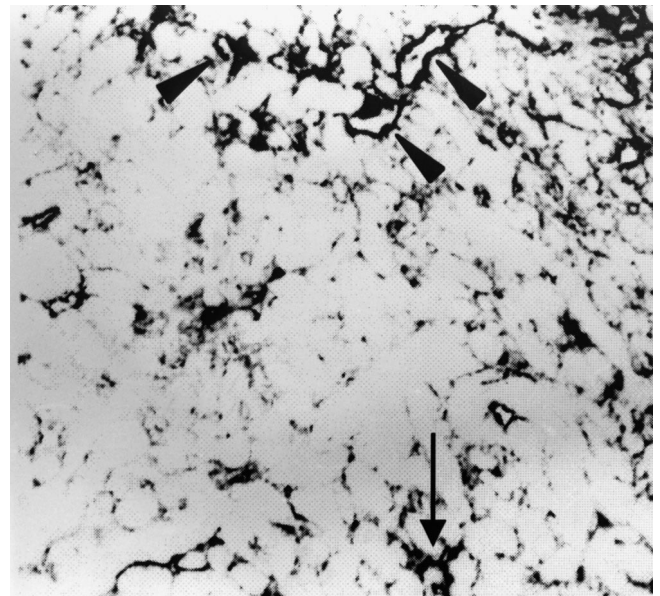

FIGURE 5. Visualization of HT-29[par] tumor vasculature basement membranes by antilaminin immunohistochemistry. Tumors grown in SCID mice show numerous blood vessels in their periphery (arrowheads) but very few in their center (arrow). Original magnification, ×450.
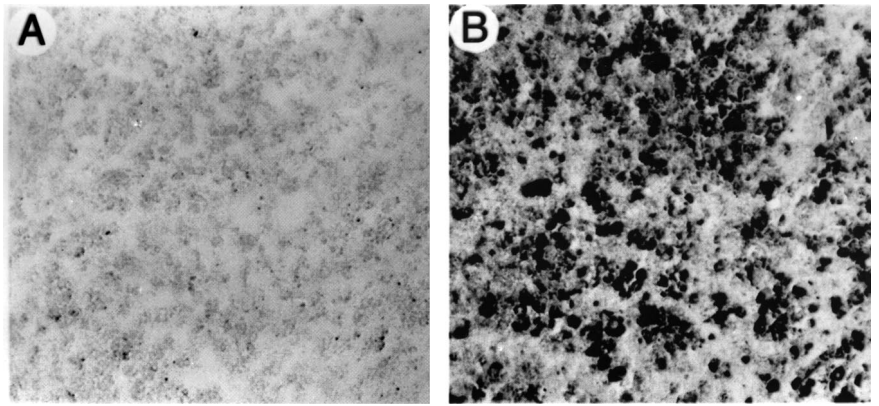
FIGURE 6. Immunohistochemic demonstration of P-gp expression in xenografts grown in SCID mice. Note absence of label in HT-29^{par} (A) and positive staining in HT-29^{mdr1} (B) tumors. Original magnification, ×450.

To exclude other conceivable mechanisms of reduced dye accumulation, that is, reduced permeability of the cell membrane and reduced binding of the dye to the intracellular targets, we inhibited the MDR efflux pump by Tween 80 (*15*), which leads to a cessation of Rhodamine 123 efflux and accumulation of the dye inside the cell. HT-29^{mdr1} cells incubated with Rhodamine 123 in the presence of Tween 80 are brightly fluorescent, confirming that the decreased fluorescence of HT-29^{mdr1} cells is indeed mainly caused by the presence of the MDR efflux pump.

Another, even more clinically relevant, substrate of the P-gp transporter pump, ^{99m}Tc-MIBI, was used in our study as a quantitative measure of MDR function. Unidirectional uptake of ^{99m}Tc-MIBI is driven thermodynamically by negative plasma membrane potentials and mitochondrial inner matrix potentials, thereby concentrating the agent within the cells in a manner similar to that of other lipophilic cationic probes of membrane potential (*4*). ^{99m}Tc-MIBI uptake is linearly related to cell number and is proportional to the extracellular concentration of ^{99m}Tc-MIBI over a range of 4–2800 pmol/L (*17*). The total concentration of Tc-MIBI (i.e., a mixture of ^{99}Tc-MIBI and ^{99m}Tc-MIBI as obtained from the ^{99}Mo/^{99m}Tc generator) administered in our study (20 pmol/10^6cells) is within this range. Kinetic studies show that ^{99m}Tc-MIBI uptake approaches a plateau at 30 min and reaches a maximum level of uptake at 1 h, which it maintained for at least 3 h thereafter (*17*). Similar results have

been obtained in our studies. In vitro ^{99m}Tc-MIBI uptake varies between different tumor cell lines. A range from 5% of the activity in the external medium in the differentiated human hepatocellular carcinoma to 28% in the human breast carcinoma cell line BT-20 has been reported (*17*). ^{99m}Tc-MIBI uptake in our nonresistant HT-29^{par} colon carcinoma cells is 0.4% of the activity of the external medium, which is a very low percentage when compared with other tumor cell lines.

Being a substrate of the P-gp efflux pump, ^{99m}Tc-MIBI is actively transported out from MDR cell lines (*4*). Enhanced extrusion results in reduced ^{99m}Tc-MIBI accumulation in chemoresistant cells by 10- to 200-fold, thereby allowing detection of the MDR phenotype. Our observations that ^{99m}Tc-MIBI uptake by HT-29^{mdr1} cells is about 8 times lower than that of HT-29^{par} cells is in accordance with these results. Because ^{99m}Tc-MIBI is an established tracer for scintigraphy, it has the potential of imaging P-gp in vivo, thereby predicting the outcome of chemotherapy (*6,7,9,21,30*). In fact, ^{99m}Tc-MIBI has been used successfully to visualize P-gp–mediated efflux in an animal tumor model (*4*). One major drawback in this study was the finding that even nonresistant HT-29^{par} tumors grown in SCID mice could not be detected by ^{99m}Tc-MIBI scintigraphy. Tumors were not visible 15 or 60 min after ^{99m}Tc-MIBI injection, which is within the usual time frame reported for ^{99m}Tc-MIBI scintigraphy (*4,6,21*). Several mechanisms underlying this un-
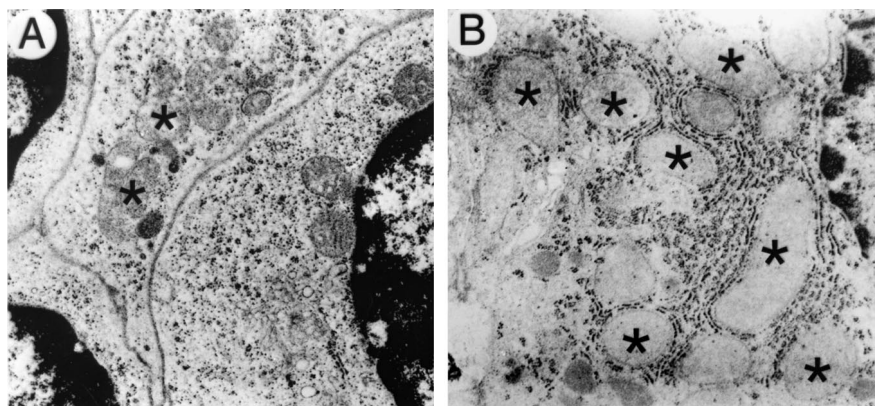

FIGURE 7. Electron micrographs of HT-29^{par} xenografted tumor cells (A) and SCID mouse hepatocyte (B). Note paucity of mitochondria (asterisks) in HT-29^{par} tumor cells and their abundance in SCID mouse hepatocytes. Original magnification, ×18,000.

expected observation are conceivable. Lack of viable tumor cells cannot account for the negative imaging results, because HT-29[par] tumors were clearly visible in FDG PET. Another reason to consider is poor tumor vasculature, because ^{99m}Tc-MIBI uptake is dependent on sufficient blood supply (20). The relatively low density in blood vessels observed histologically in HT-29[par] tumors may therefore contribute to the negative imaging. However, the low percentage ^{99m}Tc-MIBI uptake by HT-29[par] tumor cells observed in vitro before implantation into SCID mice indicates that tracer accumulation by the nonresistant tumor cells themselves is not high enough to allow detection by scintigraphy. Successful scintigraphic imaging has been reported mainly in breast cancer (9,31). Cell lines derived from this tumor show a high ^{99m}Tc-MIBI uptake in vitro (17). Clinical data based on a heterogeneous group of tumors are, however, difficult to compare with defined tumor cell lines, because ^{99m}Tc-MIBI uptake is influenced markedly by the histologic type of the cancer (31). The only study comparing ^{99m}Tc-MIBI uptake of cultured cells with that of tumors grown in nude mice (4) examines different cell lines in vitro and in vivo. The poor ^{99m}Tc-MIBI uptake by HT-29[par] tumor cells may be attributable to P-gp expression by this nonresistant cell line. This explanation is unlikely, however, because we did not observe positive JSB-1 immunoreaction in vitro or in the solid HT-29[par] tumors grown in SCID mice. However, different cellular resistance mechanisms other than P-gp expression, which have been discussed for colorectal cancer (32), cannot be excluded, for example, MDR-associated protein expression (5,26).

Because ^{99m}Tc-MIBI uptake is dependent mainly on the electrostatic gradient of mitochondrial membranes and ^{99m}Tc-MIBI therefore accumulates in tissues rich in mitochondria (16), we believe that the scarcity of mitochondria is one of the principal reasons for poor tracer uptake. Very few mitochondria have been observed in electron micrographs of cultured HT-29[par] tumor cells (33). This study shows that the mitochondrial density of HT-29[par] cells in solid tumors grown in vivo is much lower than that of hepatocytes of the SCID liver, which shows high ^{99m}Tc-MIBI uptake in scintigraphy. This assumption is also corroborated by our measurements of [201]TlCl uptake. Being 1.4% of the activity in the external medium, the accumulation of [201]TlCl, which also distributes across mitochondrial membranes (34) but is not a substrate of the P-gp transporter, has also been relatively low compared with 5% reported for other tumor cell lines (35). Our results show that sufficient ^{99m}Tc-MIBI uptake by nonresistant cells, which is related to their content of mitochondria, is the major prerequisite for successfully distinguishing between MDR and drug-sensitive cells. Thus, negative ^{99m}Tc-MIBI scintigrams are not necessarily associated with P-gp expression.

One unexpected finding of this study was the reduced FDG uptake of HT-29[mdr1] tumor cells compared with HT-29[par] cells observed in PET studies. Up to now, PET studies designed to diagnose MDR in vivo have used radiolabeled substrates of the P-gp transporter, for example, colchicine (36), verapamil (30), and daunorubicin (30). The only study examining MDR tumors using FDG (36), although describing a decreased ^{11}C-colchicine uptake in drug-resistant human neuroblastoma xenografts, does not report any differences in FDG accumulation. The decreased FDG accumulation observed in our study is not attributable to differences in tumor volume, because care was taken to let tumors grow to approximately the same size. It also cannot be explained by a larger central necrosis, which could be excluded by our histologic analysis. It is also unlikely that diminished FDG uptake of HT-29[mdr1] tumor cells is caused by decreased energy metabolism. The P-gp transporter is a drug efflux pump dependent on adenosine triphosphate, bringing about greater energy demand by MDR cells (37). In fact, MDR is associated with an elevated rate of glycolysis (38) and a higher glucose requirement (39). Therefore, it seems most likely that FDG accumulation is reduced because of an altered glucose transport into HT-29[mdr1] tumor cells. Plasma membrane glucose transporter GLUT-1 levels are known to be diminished progressively with elevated P-gp levels (37). This result may also lead to reduced FDG uptake visible in PET imaging. Moreover, differences in glucose metabolism have been described in MDR cell lines (40), which may contribute to decreased FDG accumulation. Our results indicate that FDG PET may therefore be a potential marker for detecting P-gp in vivo. A systematic analysis of FDG accumulation by HT-29[par] and HT-29[mdr1] tumor cells in vitro and in vivo is currently in process.

CONCLUSION

In this study, P-gp expression of nonresistant and MDR HT-29 human colon carcinoma cell lines was determined systematically both in vitro by immunohistochemic and functional assays and in vivo by functional imaging using ^{99m}Tc-MIBI scintigraphy and FDG PET of the same carcinoma cells growing in SCID mice. Results were compared with histologic and electron microscopic analyses of the xenografted tumors. Our results show that sufficient ^{99m}Tc-MIBI uptake by nonresistant cells, which is related to their content of mitochondria, is the major prerequisite for successfully distinguishing between MDR and drug-sensitive cells. Thus, negative ^{99m}Tc-MIBI scintigrams are not necessarily associated with P-gp expression. In some tumors, FDG PET may be an in vivo marker for MDR.

REFERENCES

1. Wadkins RM, Roepe PD. Biophysical aspects of P-glycoprotein-mediated multidrug resistance. *Int Rev Cytol.* 1997;171:121–165.

2. Eytan GD, Kuchel PW. Mechanism of action of P-glycoprotein in relation to passive membrane permeation. *Int Rev Cytol*. 1999;190:175–250.

3. Gottesman MM. How cancer cells evade chemotherapy: sixteenth Richard and Hinda Rosenthal Foundation Award lecture. *Cancer Res*. 1993;53:747–754.

4. Piwnica WD, Chiu ML, Budding M, Kronauge JF, Kramer RA, Croop JM. Functional imaging of multidrug-resistant P-glycoprotein with an organotechnetium complex. *Cancer Res*. 1993;53:977–984.

5. Hendrikse NH, Franssen EJ, Van der Graaf WT, et al. ^{99m}Tc-sestamibi is a substrate for P-glycoprotein and the multidrug resistance-associated protein. *Br J Cancer*. 1998;77:353–358.

6. Kao CH, ChangLai SP, Chieng PU, Yen TC. Technetium-99m methoxyisobutylisonitrile chest imaging of small cell lung carcinoma: relation to patient prognosis and chemotherapy response—a preliminary report. *Cancer*. 1998;83:64–68.

7. Bom HS, Kim YC, Song HC, Min JJ, Kim JY, Park KO. Technetium-99m-MIBI uptake in small cell lung cancer. *J Nucl Med*. 1998;39:91–94.

8. Yokogami K, Kawano H, Moriyama T, et al. Application of SPET using technetium-99m sestamibi in brain tumours and comparison with expression of the MDR-1 gene: is it possible to predict the response to chemotherapy in patients with gliomas by means of ^{99m}Tc-sestamibi SPET? *Eur J Nucl Med*. 1998;25:401–409.

9. Fujii H, Nakamura K, Kubo A, et al. ^{99m}Tc-MIBI scintigraphy as an indicator of the chemosensitivity of anthracyclines in patients with breast cancer. *Anticancer Res*. 1998;18:4601–4605.

10. Breuer W, Slotki IN, Ausiello DA, Cabantchik IZ. Induction of multidrug resistance downregulates the expression of CFTR in colon epithelial cells. *Am J Physiol*. 1993;265:C1711–C1715.

11. Kunzelmann K, Slotki IN, Klein P, et al. Effects of P-glycoprotein expression on cyclic AMP and volume-activated ion fluxes and conductances in HT-29 colon adenocarcinoma cells. *J Cell Physiol*. 1994;161:393–406.

12. Ambasch K, Cabantchik ZI, Slotki IN. Effects of hypotonic and hypoionic media on drug pumping by P-glycoprotein expressed in epithelial and nonepithelial cell lines. *J Cell Physiol*. 1995;164:117–122.

13. Schumacher U, Mitchell BS. Use of clinically relevant human–SCID-mouse models in metastasis research [letter]. *Trends Biotechnol*. 1997;15:239–241.

14. Mitchell BS, Horny HP, Adam E, Schumacher U. Immunophenotype of human HT29 colon cancer cell metastases in the lungs of SCID mice: spontaneous versus artificial metastases. *Invasion Metastasis*. 1997;17:75–81.

15. Neyfakh AA. Use of fluorescent dyes as molecular probes for the study of multidrug resistance. *Exp Cell Res*. 1988;174:168–176.

16. Piwnica WD, Kronauge JF, Chiu ML. Uptake and retention of hexakis (2-methoxyisobutyl isonitrile) technetium(I) in cultured chick myocardial cells. Mitochondrial and plasma membrane potential dependence. *Circulation*. 1990;82:1826–1838.

17. Delmon-Moingeon LI, Piwnica WD, Van den Abbeele AD, Holman BL, Davison A, Jones AG. Uptake of the cation hexakis(2-methoxyisobutylisonitrile)-technetium-99m by human carcinoma cell lines in vitro. *Cancer Res*. 1990;50:2198–2202.

18. Pavelic ZP, Sever Z, Fontaine RN, et al. Detection of P-glycoprotein with JSB-1 monoclonal antibody in B-5 fixed and paraffin-embedded cell lines and tissues. *Sel Cancer Ther*. 1991;7:49–58.

19. Tapiero H, Munck JN, Fourcade A, Lampidis TJ. Cross-resistance to Rhodamine 123 in Adriamycin- and daunorubicin-resistant Friend leukemia cell variants. *Cancer Res*. 1984;44:5544–5549.

20. Kostakoglu L, Kiratli P, Ruacan S, et al. Association of tumor washout rates and accumulation of technetium-99m-MIBI with expression of P-glycoprotein in lung cancer. *J Nucl Med*. 1998;39:228–234.

21. Sun S-S, Hsieh J-F, Tsai S-C, Ho Y-J, Lee J-K, Kao C-H. Expression of mediated P-glycoprotein multidrug resistance related to Tc-99m MIBI scintimammography results. *Cancer Lett*. 2000;153:95–100.

22. Kawasaki M, Nakanishi Y, Kuwano K, Takayama K, Kiyohara C, Hara N. Immunohistochemically detected p53 and P-glycoprotein predict the response to chemotherapy in lung cancer. *Eur J Cancer*. 1998;34:1352–1357.

23. Spoelstra EC, Dekker H, Schuurhuis GJ, Broxterman HJ, Lankelma J. P-glycoprotein drug efflux pump involved in the mechanisms of intrinsic drug resistance in various colon cancer cell lines. Evidence for a saturation of active daunorubicin transport. *Biochem Pharmacol*. 1991;41:349–359.

24. Roninson IB. The role of the MDR1 (P-glycoprotein) gene in multidrug resistance in vitro and in vivo. *Biochem Pharmacol*. 1992;43:95–102.

25. Lee JS, Paull K, Alvarez M, et al. Rhodamine efflux patterns predict P-glycoprotein substrates in the National Cancer Institute drug screen. *Mol Pharmacol*. 1994;46:627–638.

26. Vergote J, Moretti JL, de Vries EG, Garnier SA. Comparison of the kinetics of active efflux of ^{99m}Tc-MIBI in cells with P-glycoprotein-mediated and multidrug-resistance protein-associated multidrug-resistance phenotypes. *Eur J Biochem*. 1998;252:140–146.

27. Weaver JL, McKinney L, Schoenlein PV, Goldenberg S, Gottesman MM, Aszalos A. MDR1/P-glycoprotein function. I. Effect of hypotonicity and inhibitors on Rhodamine 123 exclusion. *Am J Physiol*. 1996;270:C1447–C1452.

28. Muller MR, Lennartz K, Baack B, Heim MM, Seeber S, Scheulen ME. Simultaneous measurement of cellular P-glycoprotein content and function by multiparametric flow-cytometry. *Int J Clin Pharmacol Ther*. 2000;38:180–186.

29. Kobayashi H, Takemura Y, Kawai Y, et al. Competitive reverse transcription-polymerase chain reaction assay for quantification of human multidrug resistance 1 (MDR1) gene expression in fresh leukemic cells. *J Lab Clin Med*. 2000;135:199–209.

30. Hendrikse NH, Franssen EJ, Van der Graaf WT, Vaalburg W, de Vries EG. Visualization of multidrug resistance in vivo. *Eur J Nucl Med*. 1999;26:283–293.

31. Buscombe JR, Cwikla JB, Thakrar DS, Hilson AJ. Uptake of Tc-99m MIBI related to tumour size and type. *Anticancer Res*. 1997;17:1693–1694.

32. Linn SC, Giaccone G. MDR1/P-glycoprotein expression in colorectal cancer. *Eur J Cancer*. 1995;31A:1291–1294.

33. Prat F, Chapelon JY, Chauffert B, Ponchon T, Cathignol D. Cytotoxic effects of acoustic cavitation on HT-29 cells and a rat peritoneal carcinomatosis in vitro. *Cancer Res*. 991;51:3024–3029.

34. Saris NE, Skulskii IA, Savina MV, Glasunov VV. Mechanism of mitochondrial transport of thallous ions. *J Bioenerg Biomembr*. 1981;13:51–59.

35. Maublant JC, Zhang Z, Rapp M, Ollier M, Michelot J, Veyre A. In vitro uptake of technetium-99m-teboroxime in carcinoma cell lines and normal cells: comparison with technetium-99m-sestamibi and thallium-201. *J Nucl Med*. 1993;34:1949–1952.

36. Levchenko A, Mehta BM, Lee JB, et al. Evaluation of ^{11}C-colchicine for PET imaging of multiple drug resistance. *J Nucl Med*. 2000;41:493–501.

37. Bentley J, Quinn DM, Pitman RS, Warr JR, Kellett GL. The human KB multidrug-resistant cell line KB-C1 is hypersensitive to inhibitors of glycosylation. *Cancer Lett*. 1997;115:221–227.

38. Bell SE, Quinn DM, Kellett GL, Warr JR. 2-Deoxy-D-glucose preferentially kills multidrug-resistant human KB carcinoma cell lines by apoptosis. *Br J Cancer*. 1998;78:1464–1470.

39. Stein WD, Cardarelli C, Pastan I, Gottesman MM. Kinetic evidence suggesting that the multidrug transporter differentially handles influx and efflux of its substrates. *Mol Pharmacol*. 1994;45:763–772.

40. Ferretti A, Chen LL, Di Vito M, et al. Pentose phosphate pathway alterations in multi-drug resistant leukemic T-cells: 31P NMR and enzymatic studies. *Anticancer Res*. 1993;13:867–872.